Electrochimica Acta 235 (2017) 480–487

Contents lists available at ScienceDirect

Electrochimica Acta

journal homepage: www.elsevier.com/locate/electacta

Microwave-Electrochemical Deposition of a Fe-Co Alloy with Catalytic Ability in Hydrogen Evolution

Gema Cabello[a,*], Murilo F. Gromboni[a,*], Ernesto C. Pereira[a], Lucia H. Mascaro[a], Frank Marken[b]

[a] Department of Chemistry, Universidade Federal de São Carlos, São Carlos 13565-905, SP, Brazil
[b] Department of Chemistry, University of Bath, Claverton Down, Bath BA2 7AY, UK

ARTICLE INFO

Article history:
Received 22 December 2016
Received in revised form 14 March 2017
Accepted 15 March 2017
Available online 19 March 2017

Keywords:
microwave-assisted electrodeposition
hydrogen evolution reaction
iron-cobalt nano-alloy
electrocatalyst

ABSTRACT

A novel microwave-electrochemical process is shown to allow Fe-Co alloy to be formed at a stainless steel electrode under fast mass transport – high temperature deposition conditions. In contrast to the Fe-Co alloy formed under ambient conditions, the microwave Fe-Co alloy is produced with a Fe:Co ratio close to unity (mass transport controlled deposition). Unusual properties of the new alloy material include good electrocatalytic performance for the hydrogen evolution reaction (HER), showing low onset overpotential (145 mV), high exchange current density (20 mA cm^{-2}) and Tafel parameters close to those for Pt on stainless steel. It is suggested that in future the microwave-electrochemical deposition method can help providing novel sustainable alloy catalyst materials for a wider range of applications.

1. Introduction

Electrochemical production of hydrogen from water using robust, efficient and sustainable catalysts materials remains an important challenge in the field of renewable energies. An advanced HER catalyst material should be able to operate at low overpotential while generating large cathodic currents. Pt-group metals generally show the highest activity toward the hydrogen evolution reaction (HER) but, replacing them with earth abundant metals is highly desirable. Although most of the transition metals have been tested as potential catalysts for the HER [1], there are still opportunities in exploiting novel alloys formed under unusual high temperature electro- formation methods. Bi- and tri-metallic alloys combining metals from the left and right branch of Balandin's volcano plot have been introduced [2,3] in order to obtain materials with a performance close to that of platinum. In particular, iron alloys have received attention [4,5] for applications in (electro-)catalysis. There have been investigations exploring Fe-Mo [6] and Co-Mo [7,8], alloys as well as FeCoNi [9,10] and FeCoSiB [11,12] type alloys. It is shown here that also alloys based on Fe and Co (both from the same side of the volcano plot) can be formed to perform as effective HER catalysts. The electrodeposition of Fe-Co alloys has been extensively studied, mainly due to their interesting magnetic properties and their applications. There are also potential applications related to printing and magnetic recording devices [13].

The need for novel sustainable catalyst materials in particular for applications where platinum is dominant (fuel cells, water electrolysers, solar fuel production, etc.) has led to numerous new materials being developed and tested. The 2D-structured transition metal dichalcogenides (e.g. MoS_2) [8,14,15] are prominent new contenders. Alloys such as Ni/Co and Ni/V [16], Ni/Mo [17,18], Co/Mo, and Co/W [19] have been reported to provide promising results. In this paper we report the microwave-electrochemical deposition of Fe-Co alloy (1:1) on a stainless steel substrate, yielding a dendritic alloy with the stoichiometric composition of the precursor solution. Preliminary tests suggest good electrocatalytic performance for the hydrogen evolution reaction (HER).

There have been considerable efforts dedicated to the application of microwave energy in the production of novel materials and in materials conversion processes [20–25]. Microwave processes are generally carried out in closed reactors and either under dry conditions [26,27] or in a liquid (super-)heated phase [28,29]. Microwave reactors usually provide a uniform field distribution either under multi-mode [30] or standing wave pattern conditions [31–33], but metal objects (electrodes) are known to distort the field pattern. Therefore, in contrast to these types of processes, a microwave-electrochemical process has been developed, in which the microwave energy is "self-focused" into a very small volume of

* Corresponding authors.
E-mail addresses: g.cabello@ufscar.br (G. Cabello), mgromboni@yahoo.com.br (M.F. Gromboni).

http://dx.doi.org/10.1016/j.electacta.2017.03.117
0013-4686/

liquid electrolyte in the vicinity of the electrode surface [34]. Usually, small diameter electrodes (or arrays of electrodes [35]) provide the most dramatic effects in terms of mass transport and localized superheating. Microelectrodes have been usually employed in microwave-assisted electrochemical processes because of the observed 'jet boiling effect', which leads to an enhanced mass transport to the electrode. However, in order to broaden these processes practical applicability, the use of electrodes with larger surface area have been successfully used, such as FTO slides with 0.5 cm^2 exposed surface area [36]; 500 μm diameter glassy carbon rod; and 500 × 500 μm^2 diamond rod [37]. On the other hand, it has been shown that arrays or assemblies of microelectrodes wired in parallel, show similar performance as macroelectrodes [38,39]. Therefore, it may be possible in future to use microwave-assisted electrodeposition for large scale and mass production of the catalyst.

Fe-Co bimetallic films with several compositions have been previously reported in the absences of microwaves [40], showing that electrodeposition is a cost-effective technique for obtaining Fe-Co alloys, although it leads to anomalous iron deposition. On the other hand, a synthesis of Fe-Co bimetallic nanoparticles based on a microwave-assisted hydrothermal route, has been shown to lead to spinel phase and small grain nanoparticles under short reaction time conditions [41]. The fabrication of electrodes to study these materials has not been reported.

Although electrodeposition processes under microwave-electrochemical conditions have been studied before [36,37,42,43], there has been no investigation of the products that are formed via microwave-electrochemical co-deposition. The massively enhanced electrodeposition rate in the presence of microwaves (up to three orders of magnitude) has been shown to lead to new morphologies by exploiting the focused stationary high temperatures and of the forced convection at the electrode-electrolyte interface [44]. However, the process has not been exploited for the formation of novel catalytically active alloys. This report addresses the microwave-electrochemical formation of Fe-Co alloy materials that could in future be employed as hydrogen evolution catalysts replacing platinum-based commercial catalysts.

2. Experimental

2.1. Chemicals

All reagents were purchased from Aldrich in the purest commercially available grade and used as received. Solutions were prepared using Milli-Q water (Millipore, 18.2 MΩ cm). Solutions used for the microwave-assisted electrodeposition were degassed within a flow-through vacuum system. Solutions were used under ambient pressure and temperature conditions and deaerated with nitrogen.

2.2. Instrumentation

Microwave-assisted electrochemical experiments were carried out with a Bio-Logic SP-300 electrochemical workstation (Bio-Logic, France) and in a domestic-modified microwave oven as reported previously [45]. A 50 μm diameter stainless steel wire (AISI 316L, Advent) embedded in epoxy resin was used as the working electrode and the auxiliary electrode was a platinum wire. All potentials were measured and reported versus a saturated calomel electrode (SCE). Potentials in polarization curves for the HER were converted to the RHE scale with the following relation: $E(RHE) = E(SCE) + 0.242 + 0.059\ pH$. The deposited alloys morphology was studied by scanned electron microscopy (SEM, ZEISS FE-SEM, Supra-35, Germany).

2.3. Microwave-Electrochemical Deposition

Electrochemical experiments were carried out under microwave irradiation by controlling the magnetron current (0, 6, 8 10 mA) in order to achieve different temperature at solution/electrode interface. The working micro-electrode was held at a cavity on the top of the microwave oven, keeping the auxiliary and reference electrodes outside. The degassed solution containing the electrolyte (0.1 M Na_2SO_4 at pH 3, adjusted with H_2SO_4) and the Fe/Co solution (2 mM $FeSO_4$ + 2 mM $CoSO_4$) were recirculated through the system by a peristaltic pump at 2 cm^3 per minute. The surface temperature $T_{electrode}$ at the stainless steel electrode exposed to microwave radiation surface was calibrated (versus microwave magnetron anode current) based on the equilibrium potential for the $Fe(CN)_6^{4-/3-}$ redox couple as described previously [45]. The solution temperature close to the electrode, $T_{solution}$, is unknown but assumed to be higher compared to $T_{electrode}$ due to the inverted temperature gradient under microwave heating conditions. The microwave-electrochemical setup used in this work was the same as previously reported [43]. Only the working electrode was placed within the microwave cavity. Positioning of the working electrode and Teflon flow cell was optimized to allow maximum microwave intensity self-focusing at the tip of the 50 μm diameter stainless steel electrode. Cyclic voltammetry and linear stripping voltammetry experiments (both at 100 mV s^{-1}) were then conducted with different applied magnetron currents (microwave power) at an electrolyte flow of 2 cm^3 per minute to avoid or minimize bulk electrolyte heating effects. The electrodeposition was carried out under potentiostatic conditions at −1.2 V for 120 s (applying 10 mA magnetron current, corresponding to $T_{electrode}$ = 390 K) and by cyclic voltammetry from −0.25 V vs. SCE to either −0.85 V, −1.0 V, or −1.2 V vs. SCE.

2.4. HER experiments

The catalytic behaviour of the as-deposited Fe-Co alloy electrode toward the HER was investigated by steady-state voltammetry at 0.5 mV s^{-1}, in a solution containing 1.0 M KOH, and at room temperature. A 600 s pre-electrolytic reduction at −1.8 V vs. SCE was performed before every measurement in order to eliminate the native oxide layer and to guarantee a highly uniform and reproducible surface. Electrodeposited Pt and Fe-Co on stainless steel electrodes (deposited in the absence microwaves) were also investigated to compare HER efficiency with the materials deposited under microwave conditions. These coatings were electrodeposited at −1.2 V vs. SCE for 600 s in a solution containing 0.5 M H_2SO_4 and 1 mM $PtCl_6^{2-}$ or in 2 mM $FeSO_4$ + 2 mM $CoSO_4$, respectively (both at pH 3).

3. Results and discussion

In a recent report [45], we have shown that iron nanoparticles are electrodeposited at stainless steel electrodes under microwave-electrochemical conditions. These iron nanoparticles were short-lived in aqueous media, but have been detected based on the characteristic stripping voltammetry responses. Here, a combination of Co(II) and Fe(II) is employed in the aqueous electrolyte to allow more inert Fe-Co alloy to be electrodeposited. This is the first study of alloy formation under microwave-electrochemical conditions and it is shown that due to the extreme conditions at the electrode surface, alloy formation leads to uniform dendritic materials with unusual properties.

3.1. Effects on Electrodeposition. Temperature and Mass Transport

In order to study the effects of electrodeposition temperature and mass transport, a voltammetric study of the electrodeposition and electro-dissolution of Fe-Co alloy was performed with a combined aqueous Fe(II) + Co(II) solution (in 0.1 M Na_2SO_4 at pH 3) under microwave-electrochemical conditions. Initially, cyclic voltammetry experiments (Fig. 1) were carried out in the absence (no MW) and then in the presence of microwaves (MW) by gradually increasing the microwave power (with magnetron anode currents of 6, 8, and 10 mA corresponding to 342 K, 370 K and 390 K electrode surface temperature). In the absence of microwave activation (Fig. 1, no MW), the cathodic current and the charge associated with stripping peaks due to electro-dissolution processes remain insignificant. With microwave activation applied, distinct peaks are observed for metal stripping (onset at ca. −0.6 V vs. SCE), with a potential peak at −0.51 V, −0.40 V and −0.31 V for magnetron anode currents of 6, 8, and 10 mA, respectively. For the Fe-Co alloy only one stripping peak is observed. Also, microwave-enhanced limiting currents for the electrochemical reduction are observed indicative of faster electrodeposition due to enhanced mass transport combined with the increased temperature [46].

3.2. Effects of Electrodeposition Potential and Time

The deposition of Fe, Co, and Fe-Co alloy was studied separately by cyclic voltammetry at 390 K and for potential ranges from −0.25 V to (A) −0.87 V, (B) −1.0 V, (C) −1.2 V vs. SCE (Fig. 2A-C). Experiments were performed with 10 mA magnetron anode current applied and with a scan rate of 100 mV s^{-1}. With a potential window reaching −0.87 V, a Co stripping peak is observed without a distinct signal for Fe. The Fe-Co alloy stripping peak appears at a potential consistent with the Co stripping peak. In Fig. 2B the potential window is extended to −1.0 V vs. SCE and now three distinct peaks are observed for Fe (onset at −0.68 V vs. SCE), for Co (onset at −0.55 V vs. SCE), and for Fe-Co (onset at −0.55 V vs. SCE). The alloy stripping and the Co stripping signals clearly exhibit the same onset potential. Increasing the potential window further to −1.2 V vs. SCE (Fig. 2C) leads to similar effects in voltammetric profiles with Fe-Co alloy showing well-defined stripping behaviour. The cathodic reduction signal for the alloy (Fig. 2C) appears additive in magnitude and linked to (i) onset of deposition during the negative going potential scan with nucleation overpotential, (ii) rise of the current to the mass transport limit, (iii) during the reverse potential scan a step consistent with the Fe stripping onset potential at −0.7 V vs. SCE (close to the reversible Fe(0/II) or stripping onset potential), and (iv) a further step consistent with the Co stripping onset potential at −0.55 V vs. SCE (close to the reversible Co(0/II) potential). Voltammetric data suggest that Fe-Co alloy undergoes oxidative stripping at the same potential where Co metal undergoes stripping, which may be linked to a Co top-layer, attributed to the deposition conditions. In this particular case, electrodeposition was not performed at a fixed potential, but by cyclic voltammetry sweeping up to different negative potentials (from −0.25 V to −0.85 V, −1.0 V and −1.2 V, Fig. 2A, B and C, respectively). This procedure leading to different composition of the deposited material depending on the negative potential achieved. First, cyclic voltammetry was performed in a potential window from −0.25 V to −0.85 V, a potential range in which only Co deposition was achieved (Fig. 2A). Co-deposition of Fe-Co took place when the potential window was increased up to −1.0 V (Fig. 2B). Under these conditions, in the reverse potential sweep, Co deposition took place again at −0.9 V, leading to a 'multilayer' electrode with a first layer formed by Co, a second layer formed by Fe-Co and a last layer with Co-rich material. The same onset potential can be observed for peaks in Fig. 2A-C, corroborating our assumption, in addition to the results obtained by linear sweep voltammetry (Fig. 2D-F), in which the electrodeposition was carried out by applying a fixed potential and different onset potential for every peak corresponding to Fe, Co and Fe-Co can be observed.

Linear sweep voltammograms were performed after 120 s deposition time at the negative end of the potential window (Fig. 2D-F). Although trends are generally consistent with those observed in cyclic voltammetry experiments (Fig. 2A-C) there appears to some variability in peak currents possibly due to the extreme conditions under microwave effects causing some loss of electro-deposit in particular for data at −1.2 V vs. SCE (Fig. 2F). In all three experiments alloy was deposited, but the highest amounts of deposit (formed in a dynamic steady state) appears to be produced at −0.87 V vs. SCE (Fig. 2D). The simultaneous formation of hydrogen gas in particular for deposition at more negative potential in combination with the extreme conditions (including cavitation [47] during microwave-enhanced electrodeposition) are likely to be linked to the lower amounts of deposits formed at more negative potentials.

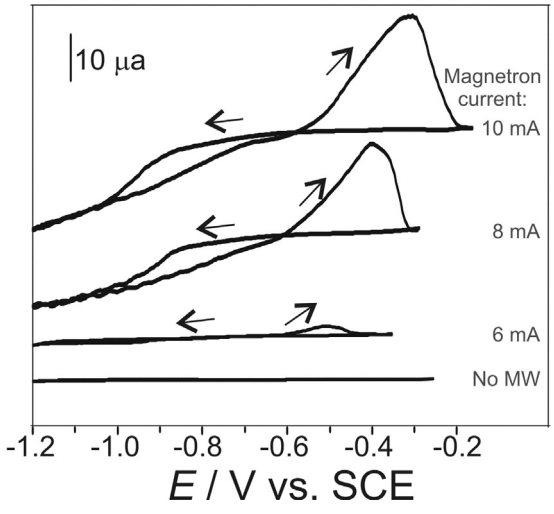

Fig. 1. Cyclic voltammograms (scan rate 100 mV s^{-1}, magnetron anode currents of 0, 6, 8 and 10 mA corresponding to ambient, 342 K, 370 K and 390 K electrode surface temperature) for the electrodeposition and stripping process in a solution containing 2 mM Fe^{2+} and 2 mM Co^{2+} in aqueous 0.1 M Na_2SO_4 at pH 3.

3.3. Characterization of Electrodeposits

Fe-Co alloy was electrodeposited potentiostatically from a solution containing 2 mM Fe^{2+} and 2 mM Co^{2+} in 0.1 M Na_2SO_4 at pH 3 onto the surface of the stainless steel electrode at −1.2 V for 120 s (applying 10 mA magnetron anode current corresponding to 390 K). Fig. 3A-D show typical SEM images for Fe-Co alloy electrodeposited under microwave conditions compared to Fe-Co alloy electrodeposited under ambient conditions (Fig. 3E). A Pt film electrodeposit (Fig. 3F) was prepared at room temperature on the same substrate, in order to compare the efficiency toward the hydrogen evolution reaction. Fig. 3A shows the deposited Fe-Co alloy completely covering the electrode surface and extending over the edges. The Fe-Co alloy deposited under microwave-electrochemical conditions exhibits well-formed dendrites (Fig. 3B) with some hierarchical order visible when going to higher magnification (Fig. 3B-C). Fig. 3C shows two clearly different structures: well-formed dendrites and a layer that is partially covering them. Higher magnification of these structures are shown in Fig. 3D. Similar structures have been previously reported to occur due to

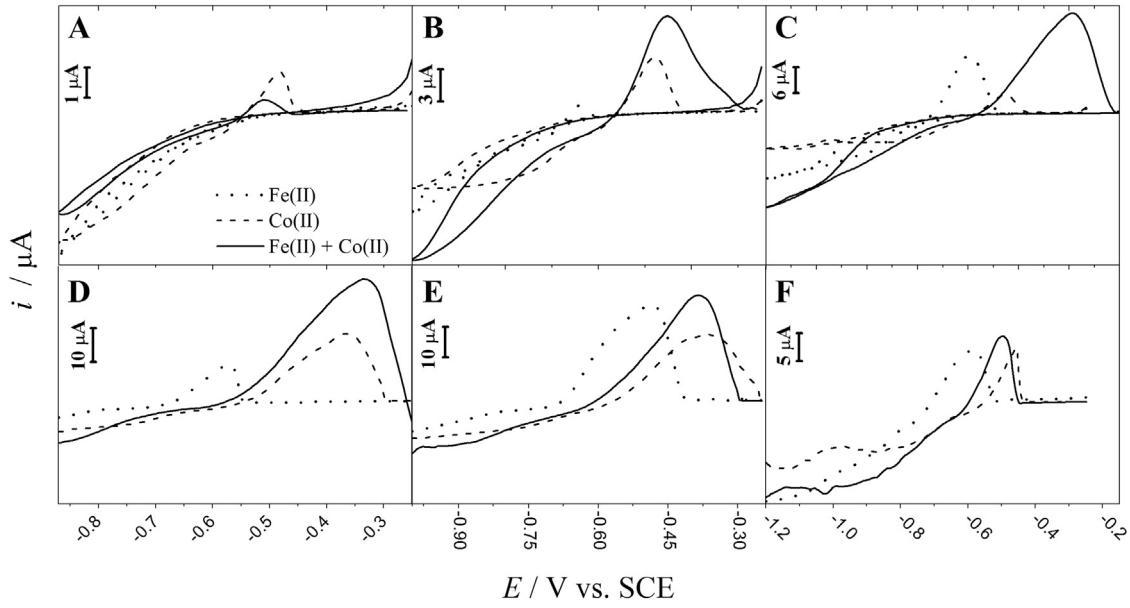

Fig. 2. Cyclic voltammograms (scan rate 100 mV s^{-1}, 10 mA magnetron current corresponding to 390 K electrode temperature) for reduction and stripping for 2 mM Fe^{2+}, 2 mM Co^{2+}, and for combined 2 mM Fe^{2+} & 2 mM Co^{2+} in aqueous 0.1 M Na_2SO_4 pH 3 employing a potential window of −0.25 V to (A) −0.87 V, (B) −1.0 V, and (C) −1.2 V vs. SCE. Also shown are linear sweep voltammograms (scan rate 50 mV s^{-1}, deposition potential (D) −0.87 V, (E) −1.0 V, (F) −1.2 V vs. SCE, 120 s deposition time).

precipitation processes of oxides/hydroxides, as in the case of NiO [48], NiOOH [49], $Ni(OH)_2$ [49] and MnO_2 [50], attributed to local variation of pH during the electrodeposition process.

Dendritic features can be valuable in materials engineering since the catalytic proprieties can be influenced by changing the size, shape, and growth orientation [51]. For comparison, the electro-deposition of Fe-Co alloy in the absence of microwaves, at ambient temperature was carried out from the same solution at the same potential but increasing the deposition time to 600 s (due to the lower deposition rate; Fig. 3E). Much less material is deposited despite of the longer deposition time and mainly the thin oxide layer is visible as platelets. There is no evidence for the

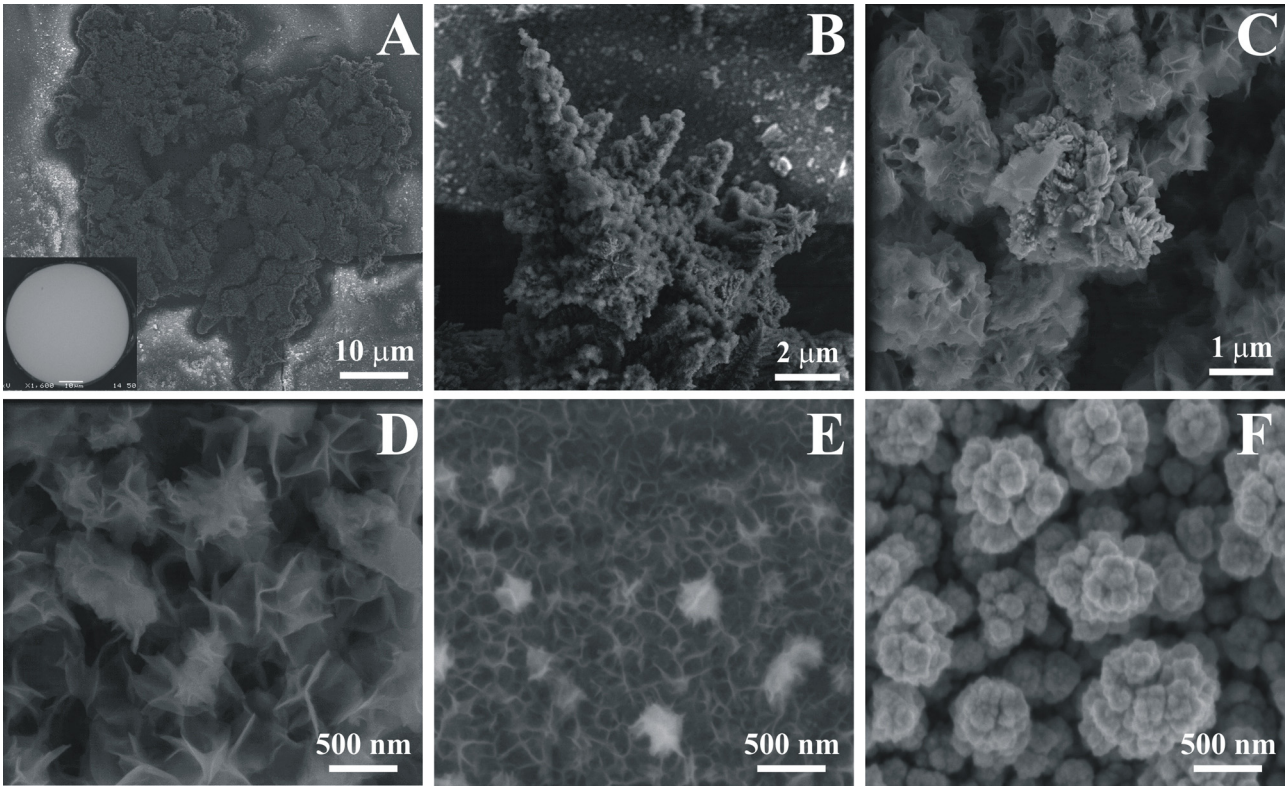

Fig. 3. (A-D) Scanning electron microscopy (SEM) images of microwave-electrochemically deposited Fe-Co alloy at −1.2 V vs. SCE for 120 s from a solution containing 2 mM Fe^{2+}, 2 mM Co^{2+}, and 0.1 M Na_2SO_4 at pH 3 (10 mA magnetron anode current corresponding to 390 K electrode surface temperature) at different magnifications (inset = polished stainless steel surface). (E) Fe-Co alloy electrodeposited under ambient conditions (in the absence of microwaves) at −1.2 V vs. SCE for 600 s. (F) Pt electrodeposited at −1.2 V vs. SCE for 600 s in a solution containing 0.5 M H_2SO_4 and 1 mM $PtCl_6^{2-}$ at pH 3.

Table 1
Composition of the Fe/Co deposits obtained from Energy Dispersive X-ray analysis (EDX) data for microwave- electrochemically deposited Fe-Co alloy at −1.2 V vs. SCE for 120 s (10 mA magnetron current corresponding to 390 K) and room temperature (no MW) electrodeposited Fe-Co at −1.2 V vs. SCE for 600 s, both in a solution containing 2 mM Fe^{2+}, 2 mM Co^{2+}, and 0.1 M Na_2SO_4 at pH 3. Data is also included for electrodeposited platinum at 0.0 V for 600 s, from a solution containing 1 mM $PtCl_6^{2-}$ in 0.5 M H_2SO_4.

	Atomic Composition (%)		
	Fe/Co (MW)	Fe/Co (no MW)	Pt
Fe	48 ± 1	62 ± 4	37 ± 9*
Co	52 ± 1	38 ± 4	–
Pt	–	–	63 ± 9

* Iron from the substrate.

dendritic alloy growth. In the case of platinum deposited in the absence of microwaves, at room temperature (Fig. 3F), the electrode surface shows a cauliflower-like growth morphology similar to that reported for other platinum on steel deposits [52].

Table 1 shows data for Energy Dispersive X-ray analysis (EDX) of the electrodeposited Fe-Co alloy obtained (A) under microwave-electrochemical conditions and (B) under ambient conditions. Differences are clearly observed in the mean values of the alloy composition electrodeposited under microwaves compared to alloy deposited in the absence of microwaves. EDX measurements were performed at different points and averaged in order to obtain an accurate value of the standard deviation (σ). The ratio of Fe:Co is clearly high in alloy obtained at ambient conditions and close to equal in alloy obtained under microwave conditions. Also, the low value of σ for material obtained under microwave conditions demonstrates a homogeneous composition across the entire electrode surface. The material deposited at room temperature shows higher dispersion and a changing composition.

Consistent with data in Table 1, co-deposition of Fe and Co into an alloy in the absence of microwaves, at room temperature, leads to a higher ratio of deposited iron due to so-called anomalous codeposition [53]. Less noble metals deposit preferentially onto the more noble ones due to a higher rate of deposition. Perhaps surprisingly, when formed under microwave conditions, Fe-Co material electrodeposits show a close to 1:1 composition (Table 1), which is explained here as a result of extremely fast deposition kinetics under microwave radiation. In addition, processes for Fe and Co deposition become mass transport controlled and therefore equally fast. This very fast deposition rate is also likely to affect the properties of the resulting alloy material. Fig. 4A shows the stripping peaks for deposits of Fe (dotted line), Co (dashed line), and Fe-Co alloy (solid line) deposited at −1.2 V for 120 s at room temperature. The amount of material deposited under these conditions is clearly much lower (2 orders of magnitude) compared to the deposition process under microwaves. In Table 2 the charge of the stripping peaks is compared to those obtained under microwave conditions.

The cyclic voltammogram for platinum deposited on the surface of the stainless steel electrode is shown in Fig. 4B. The shape of the voltammograms is in accordance with the typical features of polycrystalline platinum. The platinum oxide reduction peak is observed at the characteristic potential for bulk Pt. The hydrogen adsorption-desorption features are not well-defined but clearly present. In the case of electro-deposited platinum (Table 1), the iron found in the EDX analysis is likely to be associated mainly with the underlying stainless steel substrate. The platinum deposit is thin as can be seen in the SEM image (Fig. 3F), in which the stainless steel surface is not uniformly covered. The large dispersion in these values is also linked to this uneven morphology.

3.4. Microwave-Electrochemically Grown Fe-Co Alloy as Catalyst for the Hydrogen Evolution Reaction (HER)

New non-platinum group catalysts for hydrogen evolution are highly desirable and in particular iron alloys have received attention [4,5] for applications in (electro-)catalysis. There have been investigations exploring Fe-Mo [6] and Co-Mo [7,8], alloys as well as FeCoNi [9,10] and FeCoSiB [11,12] type alloys. Here, a preliminary attempt is reported of comparing hydrogen evolution reactivity on Fe-Co alloy for materials obtained without or with applied microwave-electrochemical conditions. The HER in 1.0 M KOH (Equation (1)) was studied and compared for the stainless steel substrate, Fe-Co alloy obtained at ambient conditions (no MW), Fe-Co alloy obtained by microwave-electrodeposition, and platinum on stainless steel.

$$2\,H_2O + 2\,e^- \rightarrow H_2 + 2\,OH^- \quad (E = 0.0\ \text{V vs. RHE, pH 14}) \qquad (1)$$

Data were obtained by steady-state voltammetry (scan rate 0.5 mV s^{-1} with 50 μm diameter electrodes) in a solution containing 1.0 M KOH at room temperature (Fig. 5). A 600 s pre-electrolytic reduction at −1.8 V vs. SCE was performed before every

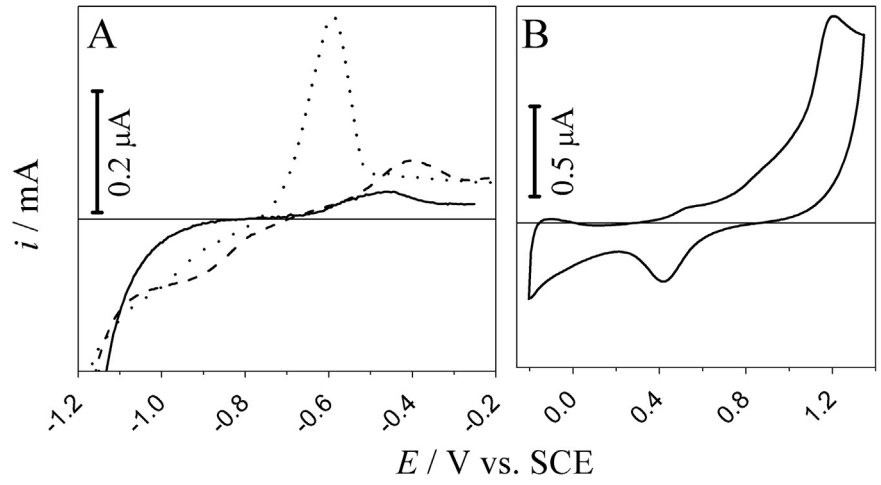

Fig. 4. (A) Linear sweep voltammetry (scan rate 50 mV s^{-1}, in a solution containing either 2 mM Fe^{2+}, 2 mM Co^{2+}, or 2 mM Fe^{2+} and 2 mM Co^{2+} in 0.1 M Na_2SO_4 at pH 3, holding the potential at −1.2 V vs. SCE for 120 s in the absence of microwaves, at room temperature) for anodic stripping of Fe (dotted line), Co (dashed line), and Fe-Co (solid line). (B) Cyclic voltammogram (scan rate 50 mV s^{-1}) for an electrodeposited platinum film on a 50 μm diameter stainless steel (film produced at 0.0 V vs. SCE for 600 s) in 0.05 M H_2SO_4.

Table 2
Calculated charge of the stripping peaks of Fe, Co and Fe/Co electrodeposited under and in the absence of microwave radiation, corresponding to Figs. 4 F and 5 A, respectively.

Stripping Peak Charge (μC)		
	MW	No MW
Fe	22	0.82
Co	11	0.15
Fe/Co	20	0.01

Table 3
HER exchange current density and Tafel parameters for the four electrodes, obtained by linear sweep voltammetry (scan rate 0.5 mV s^{-1}) in 1.0 M KOH.

	SS	Pt	Fe/Co (no MW)	Fe/Co (MW)
i_0 (mA cm^{-2})	15.3	31.1	20.4	27.0
b (mV dec^{-1})	90	60	98	68
Onset η (mV)	−350	−100	−240	−145

measurement in order to eliminate the native oxide layer and to guarantee a highly uniform and reproducible surface. The catalytic behavior of the Fe-Co alloy electrode toward the HER was compared to that for Pt as a reference electrocatalyst for the HER [54].

Polarization curves of current plotted against potential (Fig. 5A) show the HER activity of the Fe-Co (MW, solid line) electrode in comparison with the other electrodes. The Fe-Co alloy (MW) exhibited an onset overpotential near −145 mV (vs. RHE) beyond which the cathodic current exponentially increased under more negative potentials. This value is similar to that observed for Pt (−100 mV). Much more negative values were obtained for stainless steel (−350 mV) and Fe-Co (no MW, dashed line, −240 mV). In this way, we can infer that the alloy obtained under microwaves shows the enhanced activity for the HER.

The comparison between the Tafel parameters was used to confirm the high catalytic activity of the alloy. As shown in Fig. 5B, the curves follow a typical Tafel behaviour (Equation (2)).

$$\log i = -\left(\log i_0 + \left(\frac{2.303\eta}{b}\right)\right) \quad (2)$$

Here, i is the current density; i_0 is the exchange current density; b is the Tafel slope; η is the overpotential versus RHE.

The strategy to obtain high performance materials for the HER from in alkaline media has previously been based on the selection of materials with high i_0 and low b values, as well as high surface area. In addition, lower Tafel slopes together with higher exchange current densities correlate to higher hydrogen production. The Tafel slope value is an inherent property of the electrode material, giving information about the rate determining step for the HER. The hydrogen evolution reaction in alkaline media proceeds via three steps: (i) electrochemical hydrogen adsorption (Volmer reaction); (ii) electrochemical hydrogen desorption (Heyrovsky reaction) and (iii) chemical hydrogen desorption (Tafel reaction) [55]. Each reaction step shows a characteristic value for Tafel slope, being 120 mV, 40 mV and 30 mV, respectively [56]. Table 3 shows the data extrapolated from the Tafel relation for the different electrodes. The Tafel slopes for Fe-Co (MW and Pt are 68 mV dec^{-1} and 60 mV dec^{-1}, respectively, indicating the HER occurring through a Heyrovsky–Volmer mechanism, where the Heyrovsky step is rate determining [57]. When the hydrogen adsorption is the determining step, the electron transfer will be facilitated in materials with more cavities and edges due to the presence of more sites for the adsorption of hydrogen to take place. On the other hand, when the hydrogen desorption is the rate determining step the surface roughness will increase the electron transfer rate [58]. Current exchange densities can be also used to compare the activity of different catalysts. However, in most cases, it is not possible to calculate the exact surface area and instead, geometric area is used [59]. Pt and Fe-Co (MW) electrodes showed higher current densities, in good concordance with the results obtained with Tafel slopes. By contrast, the naked stainless steel and the Fe-Co (no MW) electrodes showed higher values of Tafel slope (90 and 98 mV dec^{-1}, respectively), indicating slower rates for the Volmer reaction step and, therefore, a relatively poor performance for the HER. Accordingly, the low onset potential and the small Tafel slope of 68 mV dec^{-1} confirm the large catalytic activity of the Fe-Co alloy toward the HER, close to the Tafel slope obtained for Pt. The enhanced electro-catalytic reactivity may be an effect caused by microwave-electrochemical deposition. In part, this may arise from the increased surface area (Fig. 3) although we consider the structural effects during alloy formation under very fast deposition conditions to be more significant. Further investigation may be necessary to screen a wider range of microwave-electrochemically generated alloy compositions and to include other types of alloys. Finally, improved electro-catalytically active alloys also for other types of processes (oxygen reduction, methanol oxidation, etc.) may be accessible via microwave-electrochemical deposition.

3.5. Electrode stability

Long term stability of the deposit was studied by chronoamperometry. Fig. 6A shows the change in current density with respect to time profile obtained after applying an overpotential $\eta = -250$ mV (RHE) for 6 hours in 1 M KOH. The electrode showed good performance under the applied experimental conditions, keeping ca. 88% of its initial current density after 4 h. Polarization

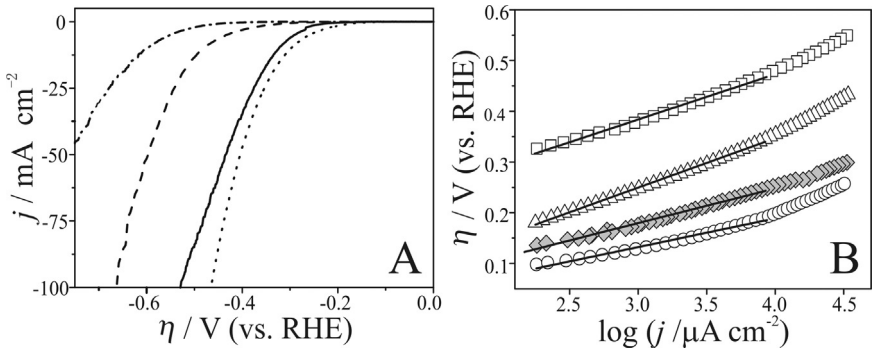

Fig. 5. (A) Linear sweep voltammetry data (after 600 s pre-electrolysis at −1.8 V vs. SCE, scan rate 0.5 mV s^{-1}) for a 50 μm diameter stainless steel bare (dashed-dotted line), with platinum (dotted line), with Fe-Co (no MW) (dashed line), and with Fe-Co deposited under microwave conditions (solid line) in aqueous 1.0 M KOH. (B) Tafel relations of the different electrodes for the HER. (□) stainless steel; (Δ) Fe-Co (no MW); (■) Fe-Co (MW); (○) Pt.

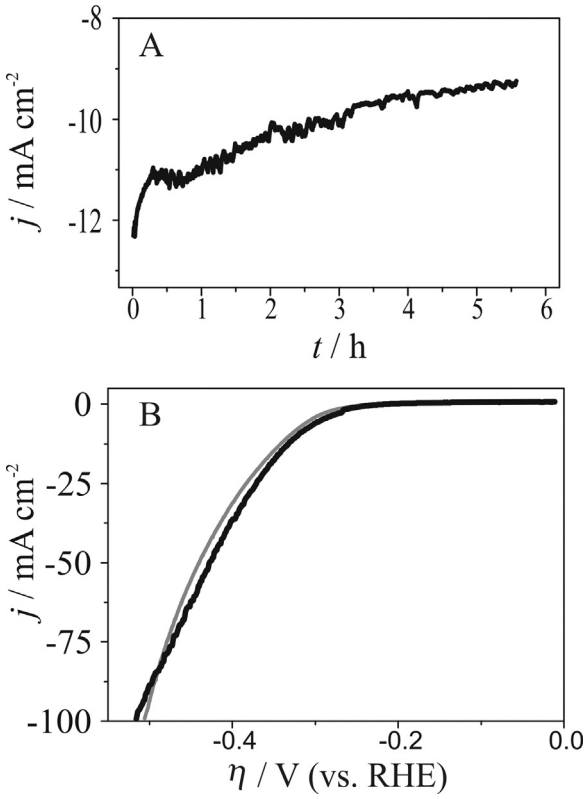

Fig. 6. (A) Chronoamperometric electrolysis carried out at η = −250 mV (RHE) for 6 h, in a solution containing 1 M KOH. (B) Polarization curves before (black) and after (grey) the stability tests, after 600 s pre-electrolysis at −1.8 V vs. SCE, scan rate 0.5 mV s^{-1}) in aqueous 1.0 M KOH.

curves performed after chronoamperometric tests (Fig. 6B, grey line) confirm the high stability of the electrode. Results were compared to those obtained previously (Fig. 6B, black line) and it can be clearly observed the electrode does not suffer severe performance degradation.

4. Conclusions

In conclusion, we have studied the effect of microwave radiation on the electro-codeposition of Fe-Co alloy and the catalytic activity of the as-grown material for the hydrogen evolution reaction. Microwave activation suppresses the anomalous deposition of iron, yielding dendrite structures with stoichiometric composition. The larger amount of Co, compared to the material obtained in the absence of microwaves, as well as the higher specific area lead to changes in the kinetic parameters of the HER approaching those of Pt (on stainless steel). Based on these preliminary findings it should be possible to explore the microwave-electrochemical alloy deposition method in more detail and to systematically develop new electrocatalyst alloys for hydrogen evolution or other applications in electrocatalysis.

Notes

The authors declare no competing financial interest.

Acknowledgements

CNPq is gratefully acknowledged for financial support under Research Project BJT-2014/400117/2014-2. LHM and FM thank CAPES (PVE 71/2013). We acknowledge FAPESP2013/07296-2 for financial support. We are much indebted to Dr. J. F. Marco for the very useful collaboration. GC and MFG gratefully acknowledge R. Camargo for SEM images acquisition and useful discussions.

References

[1] T.R. Cook, D.K. Dogutan, S.Y. Reece, Y. Surendranath, T.S. Teets, D.G. Nocera, Solar Energy Supply and Storage for the Legacy and Nonlegacy Worlds, Chem. Rev. 110 (2010) 6474–6502.
[2] Č.M. Lačnjevac, M.M. Jakšić, Synergetic electrocatalytic effects of d-metals on the hydrogen evolution reaction in industrially important electrochemical processes, Journal of the Research Institute for Catalysis Hokkaido University 31 (1983) 7–34.
[3] M.M. Jakšić, Electrocatalysis of hydrogen evolution in the light of the brewer—engel theory for bonding in metals and intermetallic phases, Electrochim. Acta 29 (1984) 1539–1550.
[4] N.R. Elezović, V.D. Jović, N.V. Krstajić, Kinetics of the hydrogen evolution reaction on Fe-Mo film deposited on mild steel support in alkaline solution, Electrochim. Acta 50 (2005) 5594–5601.
[5] G. Christou, R.V. Hageman, R.H. Holm, Hydrogen evolution from homogeneous reaction systems containing reduced molybdenum-iron-sulfur clusters, J. Am. Chem. Soc. 102 (1980) 7600–7601.
[6] A. Subramania, A.R. Sathiya Priya, V.S. Muralidharan, Electrocatalytic cobalt-molybdenum alloy deposits, Int. J. Hydrogen Energy 32 (2007) 2843–2847.
[7] H.J. Miao, D.L. Piron, Composite-coating electrodes for hydrogen evolution reaction, Electrochim. Acta 38 (1993) 1079–1085.
[8] B. Cao, G.M. Veith, J.C. Neuefeind, R.R. Adzic, P.G. Khalifah, Mixed Close-Packed Cobalt Molybdenum Nitrides as Non-noble Metal Electrocatalysts for the Hydrogen Evolution Reaction, J. Am. Chem. Soc. 135 (2013) 19186–19192.
[9] M.L. Trudeau, J.Y. Huot, R. Schulz, D. Dussault, A. Van Neste, G. L'Espérance, Nanocrystalline Fe-(Co,Ni)-Si-B: The mechanical crystallization of amorphous alloys and the effects on electrocatalytic reactions, Phys. Rev. B 45 (1992) 4626–4636.
[10] C.I. Müller, T. Rauscher, A. Schmidt, T. Schubert, T. Weißgärber, B. Kieback, L. Röntzsch, Electrochemical investigations on amorphous Fe-base alloys for alkaline water electrolysis, Int. J. Hydrogen Energy 39 (2014) 8926–8937.
[11] L. De Silva Muñoz, A. Bergel, D. Féron, R. Basséguy, Hydrogen production by electrolysis of a phosphate solution on a stainless steel cathode, Int. J. Hydrogen Energy 35 (2010) 8561–8568.
[12] M.T.M. Koper, Electrochemical Hydrogen Production Electrochemical Hydrogen Production, in: R.A. Meyers (Ed.), Encyclopedia of Sustainability Science and Technology, Springer, New York, 2012, pp. 3414–3426.
[13] E. Jean, V. Stéphane, Surface roughness and morphology of Co-(Fe and Ni) binary alloy electrodeposits studied by atomic force microscopy, J. Phys. D: Appl. Phys 32 (1999) 2342.
[14] M.A. Lukowski, A.S. Daniel, F. Meng, A. Forticaux, L. Li, S. Jin, Enhanced Hydrogen Evolution Catalysis from Chemically Exfoliated Metallic MoS_2 Nanosheets, J. Am. Chem. Soc. 135 (2013) 10274–10277.
[15] D. Kong, H. Wang, J.J. Cha, M. Pasta, K.J. Koski, J. Yao, Y. Cui, Synthesis of MoS_2 and $MoSe_2$ Films with Vertically Aligned Layers, Nano Lett. 13 (2013) 1341–1347.
[16] M.P. Marceta Kaninski, V.M. Nikolic, G.S. Tasic, Z.L. Rakocevic, Electrocatalytic activation of Ni electrode for hydrogen production by electrodeposition of Co and V species, Int. J. Hydrogen Energy 34 (2009) 703–709.
[17] J.M. Jakšić, M.V. Vojnović, N.V. Krstajić, Kinetic analysis of hydrogen evolution at Ni-Mo alloy electrodes, Electrochim. Acta 45 (2000) 4151–4158.
[18] S. Martinez, M. Metikoš-Huković, L. Valek, Electrocatalytic properties of electrodeposited Ni-15Mo cathodes for the HER in acid solutions: Synergistic electronic effect, J. Mol. Catal. A: Chem. 245 (2006) 114–121.
[19] C. Fan, D.L. Piron, A. Sleb, P. Paradis, Study of Electrodeposited Nickel-Molybdenum, Nickel-Tungsten, Cobalt-Molybdenum, and Cobalt-Tungsten as Hydrogen Electrodes in Alkaline Water Electrolysis, J. Electrochem. Soc. 141 (1994) 382–387.
[20] S. Komarneni, Q. Li, K.M. Stefansson, R. Roy, Microwave-hydrothermal processing for synthesis of electroceramic powders, J. Mater. Res. 8 (1993) 3176–3183.
[21] B.I. Kharisov, O.V. Kharissova, U. Ortiz Me'ndez, Microwave Hydrothermal and Solvothermal Processing of Materials and Compounds, in: W. Cao (Ed.), The Development and Application of Microwave Heating, 2012.
[22] V.K. Saxena, U. Chandra, Microwave Synthesis: A Physical Concept, (2011) .
[23] G.A. Tompsett, W.C. Conner, K.S. Yngvesson, Microwave Synthesis of Nanoporous Materials, ChemPhysChem 7 (2006) 296–319.
[24] I. Bilecka, M. Niederberger, Microwave chemistry for inorganic nanomaterials synthesis, Nanoscale 2 (2010) 1358–1374.
[25] M. Tsuji, M. Hashimoto, Y. Nishizawa, M. Kubokawa, T. Tsuji, Microwave-Assisted Synthesis of Metallic Nanostructures in Solution, Chemistry –A Europ. J. 11 (2005) 440–452.
[26] A. Loupy, A. Petit, M. Ramdani, C. Yvanaeff, M. Majdoub, B. Labiad, D. Villemin, The synthesis of esters under microwave irradiation using dry-media conditions, Can. J. Chem. 71 (1993) 90–95.
[27] R.S. Varma, R. Dahiya, S. Kumar, Clay catalyzed synthesis of imines and enamines under solvent-free conditions using microwave irradiation, Tetrahed. Lett. 38 (1997) 2039–2042.
[28] R. Weingarten, J. Cho, J.W.C. Conner, G.W. Huber, Kinetics of furfural production by dehydration of xylose in a biphasic reactor with microwave heating, Green Chem. 12 (2010) 1423–1429.

[29] D.P. Serrano, M.A. Uguina, R. Sanz, E. Castillo, A. Rodrı'guez, P. Sánchez, Synthesis and crystallization mechanism of zeolite TS-2 by microwave and conventional heating, Microporous Mesoporous Mater. 69 (2004) 197–208.
[30] A. Stadler, B.H. Yousefi, D. Dallinger, P. Walla, E. Van der Eycken, N. Kaval, C.O. Kappe, Scalability of Microwave-Assisted Organic Synthesis. From Single-Mode to Multimode Parallel Batch Reactors, Organic Process Research & Development 7 (2003) 707–716.
[31] H.S. Ku, F. Siu, E. Siores, J.A.R. Ball, A.S. Blicblau, Applications of fixed and variable frequency microwave (VFM) facilities in polymeric materials processing and joining, J. Mater. Process. Technol. 113 (2001) 184–188.
[32] E.K. Nyutu, C.-H. Chen, P.K. Dutta, S.L. Suib, Effect of Microwave Frequency on Hydrothermal Synthesis of Nanocrystalline Tetragonal Barium Titanate, J. Phys. Chem. C 112 (2008) 9659–9667.
[33] G.S.J. Sturm, M.D. Verweij, T. van Gerven, A.I. Stankiewicz, G.D. Stefanidis, On the effect of resonant microwave fields on temperature distribution in time and space, Int. J. Heat Mass Transfer 55 (2012) 3800–3811.
[34] I.J. Cutress, F. Marken, R.G. Compton, Microwave-Assisted Electroanalysis: A Review, Electroanalysis 21 (2009) 113–123.
[35] R.G. Compton, B.A. Coles, F. Marken, Microwave activation of electrochemical processes at microelectrodes, Chem. Commun. (1998) 2595–2596.
[36] L. Rassaei, R. Jaber, S.E. Flower, K.J. Edler, R.G. Compton, T.D. James, F. Marken, Microwave-electrochemical formation of colloidal zinc oxide at fluorine doped tin oxide electrodes, Electrochim. Acta 55 (2010) 7909–7915.
[37] M.A. Ghanem, H. Hanson, R.G. Compton, B.A. Coles, F. Marken, Microwave-enhanced electro-deposition and stripping of palladium at boron-doped diamond electrodes, Talanta 72 (2007) 66–71.
[38] S. Fletcher, M.D. Horne, Random assemblies of microelectrodes (RAM™ electrodes) for electrochemical studies, Electrochem. Commun. 1 (1999) 502–512.
[39] M.A. Ghanem, F. Marken, B.A. Coles, R.G. Compton, Microwave-enhanced electrochemical processes in micellar surfactant media, J. Solid State Electrochem. 9 (2005) 809–815.
[40] S.H. Teh, I.I. Yaacob, Synthesis and Characterization of Co-Fe Nanocrystalline Magnetic Films Electrodeposited From Electrolyte Solution Containing Sodium Saccharin, IEEE Trans. Magn. 47 (2011) 4398–4401.
[41] T. Caillot, G. Pourroy, D. Stuerga, Microwave hydrothermal flash synthesis of nanocomposites Fe-Co alloy/cobalt ferrite, J. Solid State Chem. 177 (2004) 3843–3848.
[42] F. Marken, Y.-C. Tsai, A.J. Saterlay, B.A. Coles, D. Tibbetts, K. Holt, C.H. Goeting, J. S. Foord, R.G. Compton, Microwave activation of electrochemical processes: enhanced PbO_2 electrodeposition, stripping and electrocatalysis, J. Solid State Electrochem. 5 (2001) 313–318.
[43] U. Kumar Sur, F. Marken, R.G. Compton, B.A. Coles, Microwave effects on the electrochemical deposition of copper, New J. Chem. 28 (2004) 1544–1549.
[44] A. Beckmann, B.A. Coles, R.G. Compton, P. Gründler, F. Marken, A. Neudeck, Modeling Hot Wire Electrochemistry. Coupled Heat and Mass Transport at a Directly and Continuously Heated Wire, J. Phys. Chem. B 104 (2000) 764–769.
[45] G. Cabello, M.F. Gromboni, E.C. Pereira, F. Marken, In situ microwave-enhanced electrochemical reactions at stainless steel: Nano-iron for aqueous pollutant degradation, Electrochem. Commun. 62 (2016) 48–51.
[46] F. Marken, Y.-C. Tsai, B.A. Coles, S.L. Matthews, R.G. Compton, Microwave activation of electrochemical processes: convection, thermal gradients and hot spot formation at the electrode|solution interface, New J. Chem. 24 (2000) 653–658.
[47] F. Marken, Chemical and electro-chemical applications of in situ microwave heating, Annual Reports Section C (Physical Chemistry) 104 (2008) 124–141.
[48] F. Basharat, U.A. Rana, M. Shahid, M. Serwar, Heat treatment of electrodeposited NiO films for improved catalytic water oxidation, RSC Adv. 5 (2015) 86713–86722.
[49] G. Cheng, W. Yang, C. Dong, T. Kou, Q. Bai, H. Wang, Z. Zhang, Ultrathin mesoporous NiO nanosheet-anchored 3D nickel foam as an advanced electrode for supercapacitors, J. Mater. Chem. A 3 (2015) 17469–17478.
[50] W. Wei, X. Cui, W. Chen, D.G. Ivey, Manganese oxide-based materials as electrochemical supercapacitor electrodes, Chem. Soc. Rev. 40 (2011) 1697–1721.
[51] Y. Lu, C. Beckermann, A. Karma, Convection Effects in Three-Dimensional Dendritic Growth, Mat. Res. Soc. Symp. Proc, Materials Research Society (2002) 32838.
[52] N. Zech, E.J. Podlaha, D. Landolt, Anomalous Codeposition of Iron Group Metals: I. Experimental Results, J. Electrochem. Soc. 146 (1999) 2886–2891.
[53] F. Safizadeh, E. Ghali, G. Houlachi, Electrocatalysis developments for hydrogen evolution reaction in alkaline solutions – A Review, Int. J. Hydrogen Energy 40 (2015) 256–274.
[54] T. Zerihun, P. Gründler, Electrically heated cylindrical microelectrodes. The reduction of dissolved oxygen on Pt, J. Electroanal. Chem. 404 (1996) 243–248.
[55] J.F. Walling, Electrochemical kinetics, theoretical and experimental aspects (Vetter, Klaus J.), J. Chem. Educ 45 (1968) A142.
[56] K.J. Vetter, Electrochemical Kinetics: Theoretical and Experimental Aspects, Academic Press, New York, 1967.
[57] B.E. Conway, B.V. Tilak, Interfacial processes involving electrocatalytic evolution and oxidation of H2, and the role of chemisorbed H, Electrochim. Acta 47 (2002) 3571–3594.
[58] K. Zeng, D. Zhang, Recent progress in alkaline water electrolysis for hydrogen production and applications, Prog. Energy Combust. Sci. 36 (2010) 307–326.
[59] W. Sheng, A.P. Bivens, M. Myint, Z. Zhuang, R.V. Forest, Q. Fang, J.G. Chen, Y. Yan, Non-precious metal electrocatalysts with high activity for hydrogen oxidation reaction in alkaline electrolytes, Energy Environ. Sci. 7 (2014) 1719–1724.